

# Motion on the Kaparelli fault (Greece) prior to the 1981 earthquake sequence determined from $^{36}\text{Cl}$ cosmogenic dating

L. Benedetti,<sup>1</sup> R. Finkel,<sup>1</sup> G. King,<sup>2</sup> R. Armijo,<sup>2</sup> D. Papanastassiou,<sup>3</sup> F. J. Ryerson,<sup>1</sup> F. Flerit,<sup>2</sup> D. Farber<sup>1</sup> and G. Stavrakakis<sup>3</sup>

<sup>1</sup>Lawrence Livermore National Laboratory – Institute of Geophysics and Planetary Physics, L-202, 7000 east av., CA 94550 Livermore, USA;

<sup>2</sup>Laboratoire de Tectonique, Institut de Physique du Globe de Paris, UMR 7578, 4 place Jussieu, 75252 Paris Cedex 05, France; <sup>3</sup>Institute of Geodynamics, National Observatory of Athens, PO Box 20048, Gr-118 10, Athens, Greece

## ABSTRACT

In February and March 1981, three successive destructive earthquakes occurred at the eastern end of the Gulf of Corinth. The third shock (March, 4,  $M_s \approx 6.4$ ) ruptured the Kaparelli fault. About 40 cm of a limestone fault scarp was exhumed by the earthquake. Each major prehistoric earthquake has added new surface to this cumulative scarp exposing fresh material to cosmic-ray bombardment. Using  $^{36}\text{Cl}$  cosmic ray exposure dating we have obtained the continuous exposure history for this 4–5-m-

high limestone surface at two sites about 50 m apart. The results suggest that the Kaparelli fault has ruptured three times prior to 1981 at  $20 \pm 3$  ka,  $14.5 \pm 0.5$  ka and  $10.5 \pm 0.5$  ka with slip amplitudes between 0.6 m and 2.1 m. The Kaparelli fault appears to have been inactive for 10 thousand years prior to the 1981 event.

Terra Nova, 15, 118–124, 2003

## Introduction

Although the overall relationship between active faults and plate tectonics in Greece and Turkey is now relatively well understood (Armijo *et al.*, 1996, 1999; Reilinger *et al.*, 1997; McClusky *et al.*, 2000), the long-term slip-rates of many faults and their seismic history are poorly known (Collier *et al.*, 1998). The Gulf of Corinth, a 130-km-long, E–W-orientated, north-dipping half-graben, is one of the most extensively studied features in Greece. GPS data (e.g. Briole *et al.*, 2000) and morphological studies (e.g. Armijo *et al.*, 1996) show that it is one of the most active extending regions of the world, with an opening rate of  $8\text{--}14 \text{ mm yr}^{-1}$ . This fast rate started about 1 Ma and appears to be related to the SW propagation of the North Anatolian Fault into the Aegean (Armijo *et al.*, 1999).

Detail, however, is lacking. While antithetic faulting of the downward flexed hanging-wall of the northern side of the Gulf is no more than 10% of the major faults on the southern side, total throws of many hundreds

of metres are common (Armijo *et al.*, 1996). Recent activity of those faults is generally expressed by clear limestone scarps that apparently result from successive earthquakes. Armijo *et al.* (1992) have suggested that these escarpments are generally the result of post-glacial fault slip while other workers interpret them as erosional features. In the absence of datable indicators, it has been impossible to resolve this controversy.

Exposure age dating based on the abundances of cosmogenic isotopes in exhumed earthquake scarps now provides a method for determining earthquake time-slip histories and slip-rates (cf. Zreda and Noller, 1998; Gran Mitchell *et al.*, 2001; Benedetti *et al.*, 2002). In 1981, a sequence of three earthquakes with magnitudes greater than 6 struck the area of the eastern Gulf of Corinth. (Fig. 1; Jackson *et al.*, 1982; King *et al.*, 1985). The first two events occurred during the night of 4 February at 20:53 h and of 25 February at 02:35 h, and the third one 7 days later, 4 March at 21:58 h. Their magnitudes were  $M = 6.7$ , 6.4 and 6.4 (USGS), respectively (Fig. 1). The Kaparelli fault, an antithetic fault on the north side of the Gulf of Corinth, hosted the third event of this sequence. We have applied  $^{36}\text{Cl}$  cosmic ray exposure dating to the limestone scarp that characterizes the recent movement of this fault.

## The Kaparelli fault

The first two events of the 1981 sequence occurred on the north-dipping Alepohori and Pisia faults bounding the Alkyonides Gulf (Fig. 1). All three events were associated with surface breaks (Jackson *et al.*, 1982; Hubert *et al.*, 1996). Those for Kaparelli occurred on two segments, each about 5 km long (Kaparelli-east and Kaparelli-west).

The Kaparelli-east segment lies along the southern edge of a small (385 m asl) E–W-elongated hill north of the Livadostras river. The hill slope is a smooth erosion surface composed of Mesozoic limestones and conglomerates. The long-term activity of this fault segment is expressed by the presence of multiple fresh scarps that cut the limestone bedrock and conglomerates. The main scarp segment, continuous for about 4 km, is steep,  $68\text{--}75^\circ$ , and exhibits slickensides in places (Fig. 2). The maximum height of the scarp is 4–5 m, progressively decreasing towards both extremities. Except near active gullies, there is no evidence for erosion or deposition on the hanging-wall since the scarp began to form (Fig. 2). The freshness of the Kaparelli scarp suggests that movement on the fault prior to the 1981 event is recent, probably post-glacial (Armijo *et al.*, 1992; Giraudi, 1995; Benedetti *et al.*, 2002).

Correspondence: Lucilla Benedetti, CEREGE, UMR 6635, BP 80 Europole Méditerranéen de l'Arbois, 13545 Aix en Provence Cedex 4, France. Tel.: 33 4 42 97 15 22; e-mail: benedetti@cerege.fr

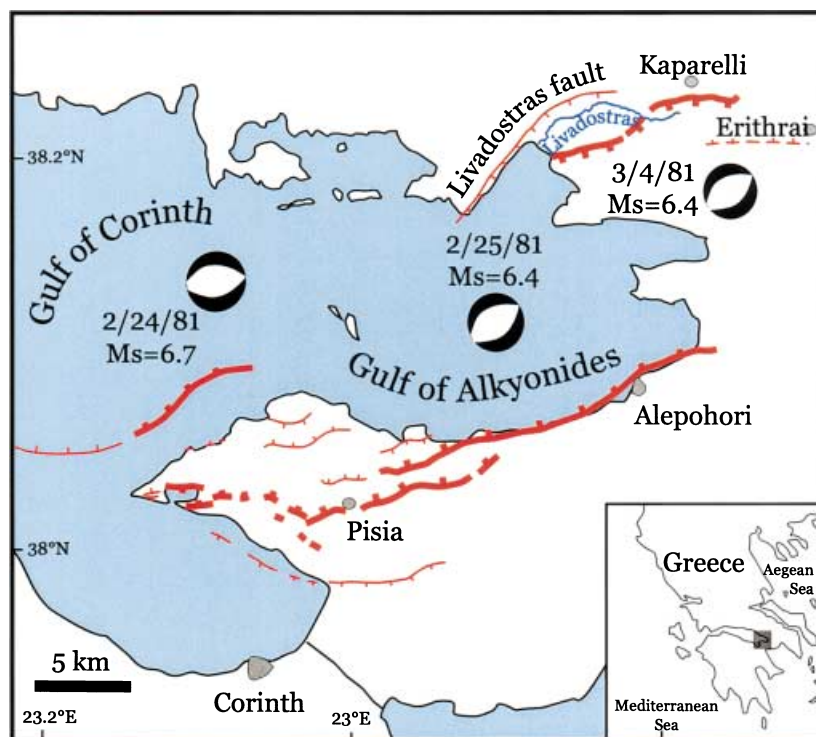


**Fig. 1** Map of the epicentral region of the 1981 Gulf of Corinth earthquake sequence, modified from Hubert *et al.* (1996). Quaternary faults are in red, with the ones known to have moved in 1981 indicated by bold lines. Earthquake fault plane solutions are from Harvard (<http://www.seismology.harvard.edu/data/>).

Along the Kaparelli-west segment, there was a scarp prior to the 1981 event. Since its maximum height is no more than 1 m, this part of the fault

could not have hosted more than one or at the most two earlier events.

The Livadostras fault (inactive in 1981), on the other hand, forms an

escarpment up to 400 m high. It lies north of the Livadostras River and constitutes an important feature that controls the morphology of the area. The Livadostras River forms a waterfall and incises bedrock and soft Quaternary sediments before reaching the Gulf of Alkyonides (Zamani *et al.*, 1981). Jackson *et al.* (1982) suggested that this dramatic rejuvenation of the river has resulted from recent motion on the Livadostras fault. The presence of ‘wineglass’ canyons also suggests that this fault has been active recently (Armijo *et al.*, 1992, 1996).

**<sup>36</sup>Cl production on the Kaparelli limestone fault scarp**

We have used <sup>36</sup>Cl cosmic ray exposure dating to assess the earthquake slip history of the Kaparelli fault by determining exposure ages as a function of height on the cumulative scarp (cf. Zreda and Noller, 1998; Gran Mitchell *et al.*, 2001; Benedetti *et al.*, 2002). <sup>36</sup>Cl is produced primarily through interactions of cosmic ray secondary neutrons and muons with Ca in the scarp limestone (CaCO<sub>3</sub>) (Stone *et al.*, 1996). The production rate decreases exponentially with depth and <sup>36</sup>Cl thus mostly accumulates after the scarp has been exhumed (Fig. 3). On an active fault, each new earthquake exposes a new section of scarp. The amount of <sup>36</sup>Cl in the scarp

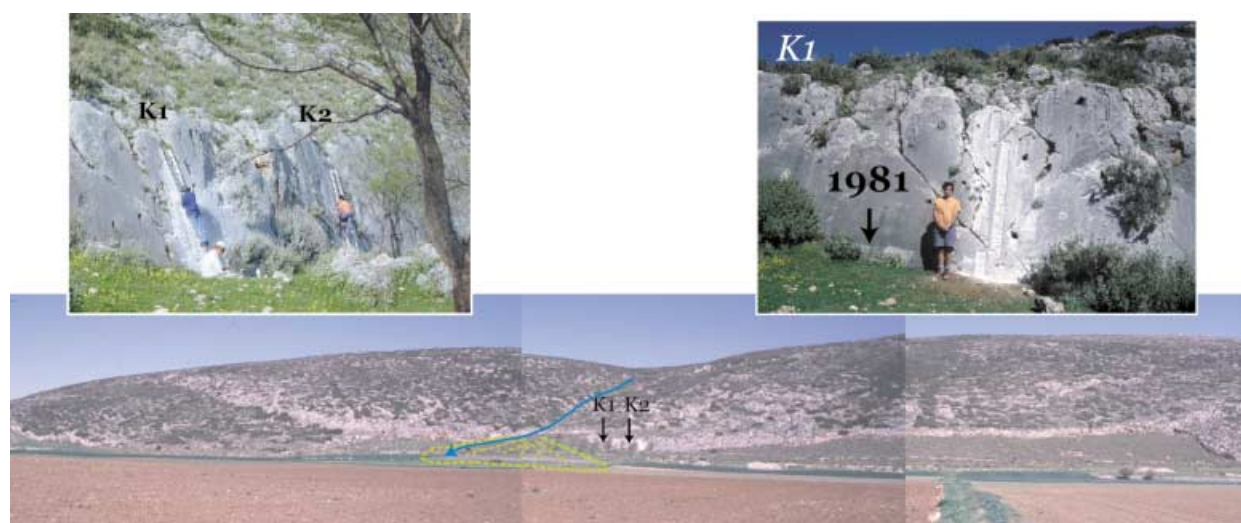


**Fig. 2** The southern segment of the Kaparelli fault with pictures of sampling sites. Note that sampling sites were chosen at sufficient distance from the alluvial fan to avoid any erosion or deposition at the base of the scarp. Samples are 15–20 cm wide, less than 2.5 cm deep. They were divided into 10-cm blocks for measurement.

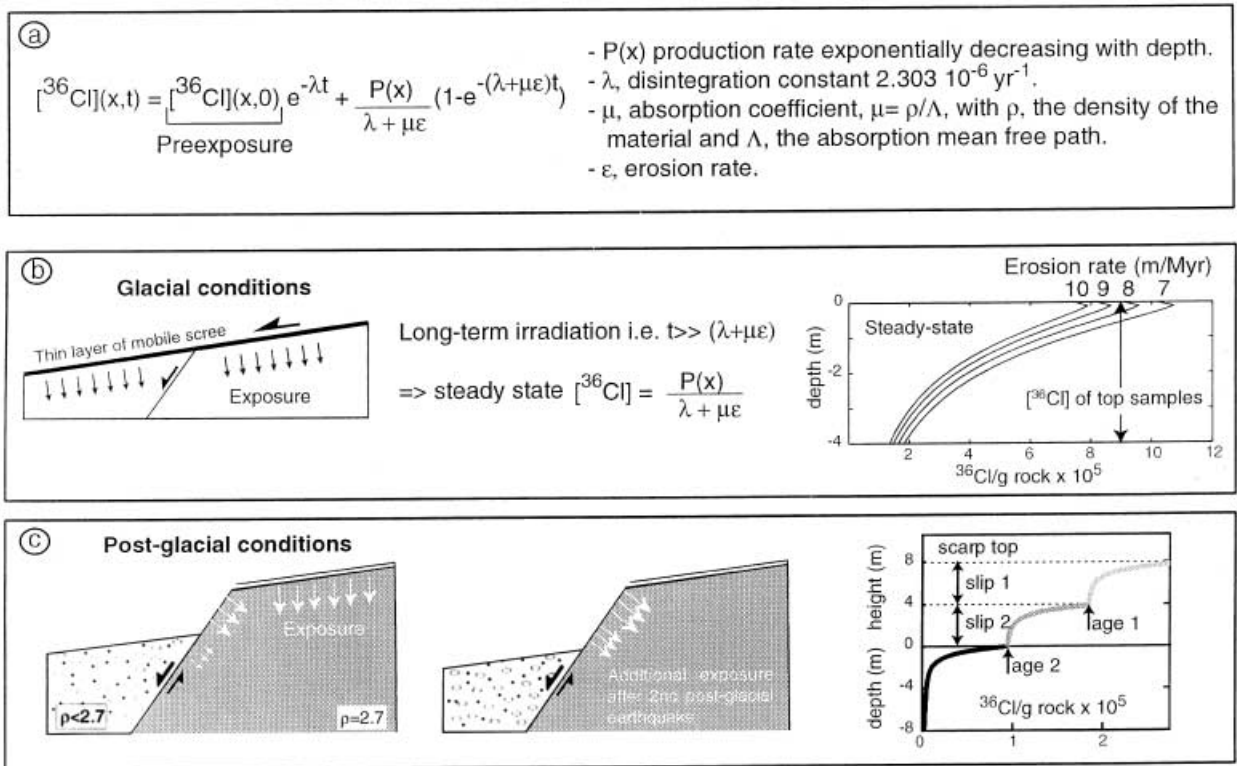


**Fig. 3** a.  $^{36}\text{Cl}$  production as a function of depth and time from Lal (1991). b. Determination of the erosion rate experienced by the footwall prior to exhumation of the scarp, during glacial conditions. The footwall surface is at steady state. An erosion rate of  $8 \text{ m Myr}^{-1}$  yields a steady-state profile with  $^{36}\text{Cl}$  concentrations of surface samples in agreement with the one collected at the top of the scarp. c. Synthetic profiles for a scarp created by two earthquakes with 4 m of slip each at 5000-year intervals. At sea level and high latitude the  $^{36}\text{Cl}$  production rate by fast neutrons is  $48.8 \pm 3.4 \text{ atoms gCa}^{-1} \text{ yr}^{-1}$  and by muons is  $2.1 \pm 0.4 \text{ atoms gCa}^{-1} \text{ yr}^{-1}$  (Stone *et al.*, 1996, 1998). Site latitude and altitude are  $38^{\circ}22'\text{N}$  and 236 m. Scaling factors for  $^{36}\text{Cl}$  production by neutrons and muons are 1.1388 and 1.0264, respectively, derived from Stone *et al.* (1996, 1998) and references therein. Dip of the fault is  $70^{\circ}\text{S}$ . Self-shielding by the scarp face is 0.61.

is the sum of  $^{36}\text{Cl}$  accumulated at depth, before the earthquake, and  $^{36}\text{Cl}$  accumulated after the earthquake, when the scarp is exposed above the surface (Fig. 3c). Since the upper parts of the scarp have been exposed longest they have the highest  $^{36}\text{Cl}$  concentrations. Concentrations decrease toward the base of the scarp.

Continuous 20-cm-wide sample profiles were collected at two locations, 10 m apart along the fault (Fig. 2). The continuous samples were divided into 10-cm sections for analysis. The  $^{36}\text{Cl}$  and chloride concentration in the carbonate was determined for 80 subsamples by isotope dilution accelerator mass spectrometry at the Lawrence Livermore National Laboratory CAMS facility (Table 1).

We compare the data to synthetic  $^{36}\text{Cl}$  profiles calculated for different faulting scenarios. In these calcula-

tions we included all sources of production: energetic neutrons, negative muon capture, capture of secondary neutrons produced by muon capture, fast muon reactions and U/Th fission (Stone *et al.*, 1998). We have assumed that no significant erosion or deposition has occurred on the hanging-wall during faulting.

To model accurately the accumulation of  $^{36}\text{Cl}$  during faulting, we need to estimate the initial  $^{36}\text{Cl}$  abundance as a function of depth prior to displacement on the fault. The footwall of the scarp consists of Mesozoic limestone that had been exposed and eroded for several millions of years prior to any movement on the fault. About a few hundred thousand years is required for a surface to reach steady-state, the exact value depending on the erosion rate, equilibrium (Fig. 3b) between the amount of  $^{36}\text{Cl}$

produced and the loss by a combination of decay and erosion (Lal, 1991). The amount of  $^{36}\text{Cl}$  accumulated on the footwall surface can be used to estimate the erosion rate of the faulted surface (Fig. 3b, Lal, 1991). Lacking this information, we used the  $^{36}\text{Cl}$  concentration of a sample collected near the top of the scarp. The  $^{36}\text{Cl}$  concentration in this sample is a lower limit to that of a sample from the upper surface. The erosion rate obtained is about  $8 \text{ m Myr}^{-1}$  (Fig. 3b); this value is a maximum bound for the erosion rate experienced by the footwall surface. The model therefore assumes that prior to faulting the surface was steadily eroding with an erosion rate of  $8 \text{ m Myr}^{-1}$ .

The attenuation length for cosmic rays depends upon the density of the target material (Lal, 1991). The higher the density is, the greater is the

**Table 1** Accelerator mass spectrometry measurements and chemical composition of samples. Blanks had consistently low  $^{36}\text{Cl}/^{37}\text{Cl}$  ratios ( $2 \times 10^{-14}$ – $8 \times 10^{-15}$ ) compared to the measured sample ratios ( $1 \times 10^{-12}$ – $6 \times 10^{-13}$ ). Replicates for  $^{36}\text{Cl}/\text{g}$  of rock reproduces within less than 3%.  $^{36}\text{Cl}$  measurements were standardized relative to an NIST  $^{36}\text{Cl}$  standard

Sample name	Height (cm)	$m_{\text{rock}}$ (g)	[Cl] p.p.m.	$^{36}\text{Cl}/^{37}\text{Cl}$ in rock	$\pm$	$^{36}\text{Cl}/\text{g}$ of rock	$\pm$
K1-3	38	36.5	19.8	6.4E-13	2.3E-14	2.6E + 05	9.4E + 03
K1-4	51	37.3	20.0	6.6E-13	2.6E-14	2.6E + 05	1.0E + 04
K1-5	62	37.0	23.4	6.9E-13	1.4E-14	2.8E + 05	5.9E + 03
K1-6	71	37.0	22.3	7.4E-13	1.8E-14	3.0E + 05	7.1E + 03
K1-7	81	36.5	22.7	7.4E-13	1.8E-14	3.2E + 05	7.9E + 03
K1-8	91	38.0	23.9	7.4E-13	1.8E-14	3.1E + 05	7.5E + 03
K1-9	101	33.1	21.2	7.5E-13	1.8E-14	3.3E + 05	7.9E + 03
K1-10	111	34.9	20.3	7.6E-13	1.8E-14	3.2E + 05	7.7E + 03
K1-11	121	36.7	21.9	8.6E-13	2.4E-14	3.3E + 05	9.6E + 03
K1-12	131	35.8	22.7	7.8E-13	3.4E-14	3.3E + 05	1.4E + 04
K1-13	141	36.2	30.2	7.4E-13	2.6E-14	3.5E + 05	1.2E + 04
K1-14	152	35.4	25.2	7.9E-13	2.5E-14	3.5E + 05	1.1E + 04
K1-15	162	38.3	20.5	9.9E-13	2.3E-14	3.8E + 05	9.1E + 03
K1-16	172	34.9	22.7	9.0E-13	2.1E-14	3.9E + 05	9.3E + 03
K1-17	185	36.6	24.3	9.7E-13	2.3E-14	4.1E + 05	9.7E + 03
K1-20	215	36.7	28.4	9.9E-13	2.4E-14	4.5E + 05	1.1E + 04
K1-21	226	39.8	28.0	1.1E-12	2.6E-14	4.5E + 05	1.1E + 04
K1-22	235	39.1	30.0	1.1E-12	2.5E-14	4.8E + 05	1.1E + 04
K1-23	245	32.9	31.0	9.9E-13	2.5E-14	5.0E + 05	1.3E + 04
K1-23B	245	24.0	32.7	7.4E-13	1.6E-14	4.8E + 05	1.1E + 04
K1-23C	245	16.4	34.3	5.3E-13	1.2E-14	4.7E + 05	1.1E + 04
K1-24	256	34.0	31.7	1.0E-12	2.2E-14	5.2E + 05	1.3E + 04
K1-25	265	35.5	32.7	1.1E-12	2.2E-14	5.2E + 05	1.2E + 04
K1-26	276	33.9	31.9	1.2E-12	3.9E-14	5.6E + 05	1.9E + 04
K1-27	289	36.2	33.0	1.2E-12	2.6E-14	5.5E + 05	1.4E + 04
K1-28	299	37.4	34.5	1.2E-12	2.7E-14	5.8E + 05	1.6E + 04
K1-29	309	34.9	29.4	1.3E-12	2.7E-14	6.1E + 05	1.3E + 04
K1-30	320	37.8	32.7	1.4E-12	3.2E-14	6.1E + 05	1.4E + 04
K1-31	329	32.9	33.8	1.3E-12	2.8E-14	6.6E + 05	1.4E + 04
K1-33	350	34.0	33.6	1.5E-12	3.2E-14	7.1E + 05	1.5E + 04
K1-34	15	35.9	26.4	6.1E-13	1.5E-14	2.7E + 05	6.5E + 03
K1-35	4	29.3	21.9	5.0E-13	1.0E-14	2.5E + 05	5.3E + 03
K6-2	25	40.1	18.7	7.5E-13	2.3E-14	2.4E + 05	7.2E + 03
K6-3	34	40.4	14.5	7.2E-13	1.8E-14	2.3E + 05	5.5E + 03
K6-4	44	39.1	18.5	6.7E-13	1.9E-14	2.2E + 05	6.3E + 03
K6-5	55	30.8	21.1	5.8E-13	1.9E-14	2.4E + 05	8.0E + 03
K6-7	75	37.5	17.7	6.5E-13	1.6E-14	2.4E + 05	5.9E + 03
K6-8	85	38.9	19.6	7.4E-13	1.8E-14	2.5E + 05	6.1E + 03
K6-9	95	38.3	18.3	6.8E-13	1.7E-14	2.5E + 05	6.4E + 03
K6-10	105	31.3	17.4	6.4E-13	1.7E-14	2.5E + 05	6.7E + 03
K6-12	125	34.8	19.1	7.8E-13	1.9E-14	2.8E + 05	7.1E + 03
K6-14	145	36.7	15.8	8.1E-13	2.0E-14	2.8E + 05	7.1E + 03
K6-15	155	33.3	21.9	7.7E-13	2.6E-14	3.1E + 05	1.0E + 04
K6-16	165	27.0	17.6	6.4E-13	1.6E-14	3.0E + 05	7.9E + 03
K6-18	185	34.9	19.7	8.6E-13	2.2E-14	3.2E + 05	8.1E + 03
K6-20	205	41.1	19.4	1.0E-12	4.3E-14	3.4E + 05	1.5E + 04
K6-21	215	41.4	20.8	9.8E-13	2.4E-14	3.3E + 05	8.2E + 03
K6-22	225	33.5	26.4	8.9E-13	2.3E-14	3.7E + 05	9.8E + 03
K6-23	236	40.2	21.5	1.1E-12	2.8E-14	3.7E + 05	8.8E + 03
K6-24	245	18.8	22.6	6.4E-13	1.6E-14	4.1E + 05	1.0E + 04
K6-25	255	41.7	21.7	1.2E-12	3.0E-14	4.0E + 05	9.9E + 03
K6-27	277	30.4	21.4	1.1E-12	2.6E-14	4.6E + 05	1.2E + 04
K6-28	288	31.6	22.2	1.2E-12	2.9E-14	4.5E + 05	1.1E + 04
K6-29	297	33.2	23.3	1.2E-12	2.9E-14	4.6E + 05	1.2E + 04
K6-30	307	36.4	24.6	1.3E-12	3.1E-14	4.6E + 05	1.1E + 04
K6-31	317	36.5	19.6	1.4E-12	3.4E-14	4.9E + 05	1.2E + 04
K6-34	348	35.6	33.9	1.4E-12	3.5E-14	6.0E + 05	1.5E + 04
K6-35	358	33.8	27.2	1.3E-12	3.4E-14	5.6E + 05	1.4E + 04
K6-36	368	36.7	38.9	1.5E-12	5.2E-14	6.9E + 05	2.4E + 04

**Table 1** (Continued)

Sample name	Height (cm)	$m_{\text{rock}}$ (g)	[Cl] p.p.m.	$^{36}\text{Cl}/^{37}\text{Cl}$ in rock	$\pm$	$^{36}\text{Cl}/\text{g}$ of rock	$\pm$
K6-37	378	34.8	26.9	1.7E-12	4.0E-14	6.8E + 05	1.6E + 04
K6-38	388	34.8	24.3	1.7E-12	4.1E-14	7.0E + 05	1.7E + 04
K6-39	398	34.5	30.4	1.6E-12	3.2E-14	7.1E + 05	1.4E + 04
K6-42	428	22.7	33.5	1.4E-12	3.3E-14	9.2E + 05	2.2E + 04

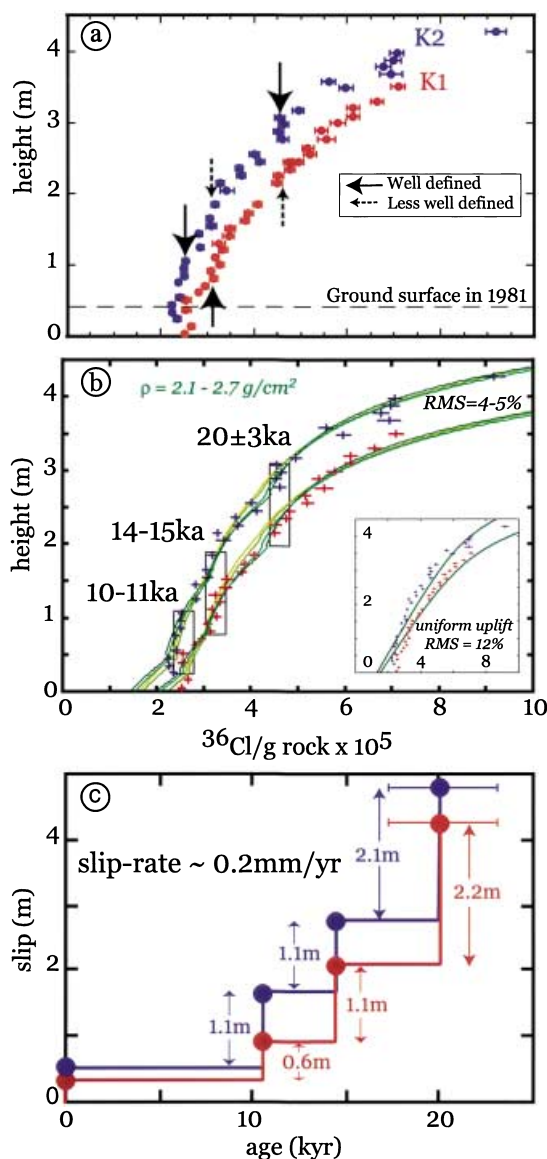


**Fig. 4** The  $^{36}\text{Cl}$  data and the models. a.  $^{36}\text{Cl}$  concentrations per gram of rock for each sample with error, blue is K2 and red K1. Arrows show discontinuities in the profile that we associated with individual earthquake events. Calcium content in the samples was measured by Atomic absorption spectrometry and was found similar in most of the samples with  $m_{\text{Ca}}/m_{\text{rock}} = 0.39 \pm 0.01$ . The contents of the other chemical elements (K, Mg, U, Th, B) were measured every 20 cm on the scarp at both sites by XRAL laboratories, Canada. b. The models. Lines are synthetic profiles for density of 2.1, 2.3, 2.5 and  $2.7 \text{ g cm}^{-3}$ , from clear green to dark green, respectively. Inset: model with a uniform uplift rate of  $0.2 \text{ mm yr}^{-1}$  yields RMS of 12% at both sites. Three earthquakes fit both sites with 4–5% RMS. c. Time per slip of event deduced from the models.

attenuation of cosmic rays and the lower the  $^{36}\text{Cl}$  production at depth (Fig. 3a). At our sampling sites, the footwall and the hanging-wall of the scarp are of two different bulk densities. The footwall is composed of limestone, with a density of  $2.7 \text{ g cm}^{-3}$  (Gosse and Phillips, 2001). The hanging-wall consists mainly of fluvial fan deposits (Fig. 2), with a lower density. To our knowledge, there are no precise estimates of the bulk density of fluvial sediments. The density of soil, about  $2 \text{ g cm}^{-3}$  (e.g. Gosse and Phillips, 2001), is a lower limit to this value. In our calculations we varied the hanging-wall density between 2.1 and  $2.7 \text{ g cm}^{-3}$ .

**Seismic history of the Kaparelli**

The  $^{36}\text{Cl}$  concentrations measured on the scarp are high ( $> 2 \times 10^5$  atoms per gram of rock). This suggests that sections of the scarp have been exposed for a long time. The  $^{36}\text{Cl}$  concentrations at K1 and K2 are homologous with two clear discontinuities in the profile and one discontinuity that is less well defined (Fig. 4a). These discontinuities are observed at the same  $^{36}\text{Cl}$  concentration – equivalent to age – on both profiles. This suggests that these discontinuities are not caused by erosional or depositional processes but by a mechanism that has affected the whole fault in the same way. We associate these discontinuities with earthquake faulting.

The two profiles were modelled independently. We tested both uniform uplift and individual earthquake models. Uniform uplift rate models yield RMS deviations that are twice those obtained for models that incorporate individual earthquakes (inset Fig. 4).

The best fit is obtained with three events of the same ages at both sites (RMS of 4–5% at K1 and K2 independently from the input density).

Although models with other earthquake times and slip amplitudes yield similar RMS values, we consider the model presented in Fig. 4(b) to be the best fit because it is the only model that (1) yields the same ages for the earthquake events at both sites, (2) is in agreement with the 1981 slip observations (Jackson *et al.*, 1982) and (3) yields reasonable values for the slip of the earlier events (Scholz, 1982).

Our synthetic profiles yield lower  $^{36}\text{Cl}$  concentrations at the base of the scarp than those we observed. This discrepancy is probably due to simplifications inherent to the model such as our consideration of only vertically penetrating muons as the source of  $^{36}\text{Cl}$  production by negative muon capture (Stone *et al.*, 1998).

Varying the hanging-wall density does not affect the quality of the fit; RMS values are similar for any density between 2.1 and 2.7 g cm $^{-3}$ . However, the higher the density, the older are the modelled ages. For example, with a hanging-wall density of 2.7 g cm $^{-3}$ , the model age for the oldest event is 23 ka whereas a density of 2.1 g cm $^{-3}$  yields an age of 17 ka. Since we cannot determine which density better fits the data, we have included this uncertainty in the error estimate for the model ages.

## Discussion and conclusions

Our results give evidence for three events at both sites at  $20 \pm 3$  ka,  $14.5 \pm 0.5$  ka and  $10.5 \pm 0.5$  ka. The time intervals between those events are 3000–9000 years, 4000–5000 years and 10 000–11 000 years, respectively. These results suggest that the Kaparelli fault had remained quiet for about 10 000 years before the 1981 earthquake.

To our knowledge this is the longest recurrence time ever demonstrated on a normal fault and shows that although normal faults might not exhibit evidence of recent movement in the form of offsets of Holocene deposits (alluvial fan or terraces), they are capable, nonetheless, of producing magnitude 6–7 earthquakes. Prior to the 1981 earthquake, the only evidence for the Quaternary activity of this fault was the presence of a limestone fault scarp. Many workers have suggested that similar escarpments in

both Italy and Greece are erosional features and are not indicators of potential earthquake hazard. The current study, combined with recent dating of the Sparta escarpment (Benedetti *et al.*, 2002), makes this view untenable. Direct fault scarp dating has important consequences for the way the seismic risk is assessed in the many parts of the central and eastern Mediterranean that are composed of predominantly limestone rocks where few potential trench sites exist for palaeoseismological assessment.

The ages in this paper were calculated using the  $^{36}\text{Cl}$  production rates from Ca of Stone *et al.* (1998) for all relevant pathways. Other published production rates (Swanson and Caffee, 2001 and references therein) are higher than the Stone *et al.* value and would lead to younger ages (by about 20%). Our results therefore confirm that the Kaparelli scarp is post-glacial, supporting the hypothesis that similar scarps elsewhere in the Mediterranean region are also post-glacial (Benedetti *et al.*, 2002).

The slip associated with the earlier events is between 0.6 m and 2.1 m, more than the  $\sim 40$  cm of average displacement observed on this fault-segment during the 1981 earthquake (Jackson *et al.*, 1982). The greater slip suggests that the length of faulting in previous events was greater (e.g. Scholz, 1982). The Kaparelli-east fault does not extend beyond the eastern extent of the 1981 rupture and the Kaparelli-west fault does not appear to extend further to the west. Furthermore, the Kaparelli-west fault has insufficient total throw to have hosted earlier large events. It therefore seems likely that the earlier events were associated with motion on the Livadostras fault. Together, the Kaparelli-east fault and the Livadostras fault are more than 30 km long.

The slip history yields an integrated slip rate of  $\sim 0.2$  mm yr $^{-1}$  which is about 10% of the rate of the main north-dipping faults on the southern side of the Gulf, but about the rate expected for antithetic faulting (e.g. Armijo *et al.*, 1996). Antithetic faults on the northern side of the Gulf of Corinth and similar faults elsewhere in the central and eastern Mediterranean are capable of hosting destructive earthquakes with magnitudes up to 7.

## Acknowledgments

This work was performed under the auspices of the US Department of Energy by University of California Lawrence Livermore National Laboratory under contract No. W-7405-Eng-48. This work has been supported by the programme PNRN and 'ACI Prevention des Catastrophes Naturelles' of INSU-CNRS contribution 331 and the EC Environment Programme (PRE-SAP). We are thankful to John Southon and Marc Caffee for assisting with the AMS measurements. We acknowledge T. Hanks, S. Pavlides and F. Phillips for their helpful reviews. This is IPGP contribution number 1866 and IGPP contribution UCRL-JC-148074.

## References

- Armijo, R., Lyon-Caen, H. and Papanastassiou, D., 1992. East-west extension and Holocene normal-faults scarps in the Hellenic arc. *Geology*, **20**, 491–494.
- Armijo, R., Meyer, B., Hubert, A. and Barka, A., 1999. Westward propagation of the North Anatolian fault into the Aegean. Timing and Kinematics. *Geology*, **27**, 267–270.
- Armijo, R., Meyer, B., King, G.C.P., Rigo, A. and Papanastassiou, D., 1996. Quaternary evolution of the Corinth Rift and its implications for the late Cenozoic evolution of the Aegean. *Geophys. J. Int.*, **126** (1), 11–53.
- Benedetti, L., Finkel, R., Papanastassiou, D., King, G., Armijo, R., Ryerson, F.J., Farber, D. and Flerit, F., 2002. Post-glacial slip history of the Sparta fault (Greece) determined by  $^{36}\text{Cl}$  cosmogenic dating: evidence for non-periodic earthquakes. *Geophys. Res. Lett.*, 10.1029/2001GL014510, 27 April 2002.
- Briole, P., Rigo, A., Lyon-Caen, H., Ruegg, J., Papazissi, K., Mitsakaki, C., Balodimou, A., Veis, G., Hatzfeld, D. and Deschamps, A., 2000. Active deformation of the Corinth rift, Greece: results from repeated Global Positioning System surveys between 1990 and 1995. *J. Geophys. Res.*, **105** (B11), 25,605–25,625.
- Collier, R., Pantosti, D., D'Addegio, G., DeMartini, P.M., Masana, E. and Sakellariou, D., 1998. Paleoseismicity of the 1981 Corinth earthquake fault: seismic contribution to extensional strain in central Greece and implications for seismic hazard. *J. Geophys. Res.*, **103** (B12), 30,001–30,019.
- Giraudi, C., 1995. Considerations of the significance of some post-glacial fault scarps in the Abruzzo Apennines (central Italy). *Quatern. Int.*, **25**, 33–45.
- Gosse, J.C. and Phillips, F.M., 2001. Terrestrial in situ cosmogenic nuclides: theory and application. *Quat. Sci. Rev.*, **20**, 1475–1560.

- Gran Mitchell, S., Matmon, A., Bierman, P.R., Enzel, Y., Caffee, M. and Rizzo, D., 2001. Displacement history of a limestone normal fault scarp, northern Israel, from cosmogenic  $^{36}\text{Cl}$ . *J. Geophys. Res.*, **106** (B3), 4247–4264.
- Hubert, A., King, G., Armijo, R., Meyer, B. and Papanastassiou, D., 1981. (1996) Fault re-activation, stress interaction and rupture propagation of the Corinth earthquake sequence. *Earth Planet. Sci. Lett.*, **142/3–4**, 573–586.
- Jackson, J.A., Gagnepain, J., Houseman, G., King, G.C., Papadimitriou, P., Soufleris, C. and Virieux, J., 1982. Seismicity, normal faulting and the geomorphological development of the Gulf of Corinth (Greece): the Corinth earthquakes of February and March 1981. *Earth Planet. Sci. Lett.*, **57**, 377–397.
- King, G.C.P., Ouyang, Z.X., Papadimitriou, P., Deschamps, A., Gagnepain, J., Housemen, G., Jackson, J., Soufleris, G. and Virieux, J., 1985. The evolution of the Gulf of Corinth (Greece): an aftershock study of the 1981 earthquakes. *Geophys. J.R. Astron. Soc.*, **80**, 677–683.
- Lal, D., 1991. Cosmic ray labeling of erosion surfaces: in situ nuclide production rates and erosion models. *Earth Planetary Sci. Lett.*, **104**, 424–439.
- McClusky, S. et al., 2000. GPS constraints on plate motion and deformation in the eastern Mediterranean: implication for plate dynamics. *J. Geophys. Res.*, **105**, 5695–5719.
- Reilinger, R., McClusky, S.C., Oral, M.B., King, R.W. and Toksoz, M.N., 1997. Global Positioning System measurements of present-day crustal movements in the Arabia-Africa-Eurasia plate collision zone. *J. Geophys. Res.*, **102**, 9983–9999.
- Scholz, C.H., 1982. Scaling laws for large earthquakes: consequences for physical models. *Bull. Seis. Soc. Am.*, **72** (1–15), 1982.
- Stone, J.O.H., Allan, G.L., Fifield, L.K. and Cresswell, R.G., 1996. Cosmogenic chlorine-36 from calcite spallation. *Geochim. Cosmochim. Acta*, **60**, 679–692.
- Stone, J.O.H., Evans, J.M., Fifield, L.K., Allan, G.L. and Cresswell, R.G., 1998. Cosmogenic chlorine-36 production in calcite by muons. *Geochim. Cosmochim. Acta*, **62**, 433–454.
- Swanson, T.W. and Caffee, M.L., 2001. Determination of  $^{36}\text{Cl}$  production rates derived from the well-dated deglaciation surfaces of Whidbey and Fidalgo Islands, Washington. *Quaternary Res.*, **56**, 366–382.
- Zamani, A., Maroukian, H. and Sabot, V., 1981. Evolution morphologique du lit central du torrent Livadostra de la region de Kaparelli (Beotie-Crece). *Ann. Geol. Pays Hell.*, **XXX/2**, 805–816.
- Zreda, M. and Noller, J., 1998. Ages of prehistoric earthquakes revealed by cosmogenic chlorine-36 in a bedrock fault scarp at Hebgen Lake. *Science*, **282**, 1097–1099.

Received 25 April 2002; revised version accepted 10 January 2003